Development of a Real-time Simulation Tool towards Self-consistent Scenario of Plasma Start-up and Sustainment on Helical Fusion Reactor FFHR-d1

T. Goto[1], J. Miyazawa[1], R. Sakamoto[1], C. Suzuki[1], R. Seki[1], S. Satake[1], B. Huang[2], M. Nunami[1], M. Yokoyama[1], A. Sagara[1] and the FFHR Design Group[1 s]

[1]National Institutes of Natural Sciences, National Institute for Fusion Science, Toki, Gifu, Japan

[2]The Graduate University of Advanced Studies, Toki, Gifu, Japan

E-mail contact of main author: goto.takuya@LHD.nifs.ac.jp

Abstract. Close investigation of plasma operation scenario for the LHD-type helical reactor FFHR-d1 in view of MHD equilibrium/stability, neo-classical/anomalous transport, alpha energy loss and impurity effect was conducted. Using a 1-D calculation model which can reproduce typical pellet discharges of LHD experiment, a self-consistent solution of plasma operation scenario was found within the operation regime that has been already confirmed in LHD experiment. The developed calculation tool enables systematic analysis of the operation regime in real time.

1. Introduction

Helical systems inherently have an advantage in a steady-state operation: no disruptive event because of a net-current-free plasma, low recirculation power because of no need of current drive. Among the helical systems, the heliotron system with two continuous helical coils has recorded remarkable achievements in the experiment of the Large Helical Device (LHD). Based on the LHD experimental achievements, conceptual design of the LHD-type helical reactor FFHR-d1 [1] has been advanced by taking advantage of the helical system and by utilizing the knowledge from the past design studies and engineering R&Ds for large-size devices including LHD and ITER. In the previous study [2], plasma operation control scenario towards steady-state self-ignition operation point was examined using the 1-D model that is based on LHD experimental observation and coupled with a couple of detailed physics analysis tools provided by the integrated transport analysis suite TASK3D [3]. Consequently, plasma startup and steady-state sustainment of self-ignition state with a fusion power of 3 GW which is consistent with MHD equilibrium and neo-classical transport was confirmed for the design point of the high magnetic field option of FFHR-d1 (hereafter this option is called as FFHR-d1B): the major radius of the helical coil winding center R_c = 15.6 m, the magnetic field strength at the helical coil winding center B_c = 5.6 T.

On the other hand, compatibility between MHD stability and good confinement is recognized as one of the crucial issues of heliotron systems like LHD. The effect of boot-strap current under a burning plasma condition has not yet been fully examined. Therefore, the 1-D calculation code has been extended to deal with these issues (i.e., MHD stability, anomalous transport and boot-strap current) and plasma operation regime of FFHR-d1B was examined in depth. Brief review of the calculation model and prerequisites of the calculation are given in

Section 2. The results of calculation are given in Section 3. Finally, these are summarized in Section 4.

2. Calculation method

2.1.Calculation model

Temporal evolution of the radial profiles of plasma density and temperature are estimated by a reduced model based on the LHD experiment. Temporal evolution of electron and ion density profiles is calculated by solving a 1D diffusion equation in cylindrical geometry:

$$\frac{\partial n_{e,i}}{\partial r} = \frac{1}{r}\frac{\partial}{\partial r}\left\{ r\left(D\frac{\partial n_{e,i}}{\partial r} - n_{e,i}V \right)\right\} + S\,. \quad (1)$$

Based on the LHD experimental observation, no convection flow (V = 0) and spatially constant diffusion coefficient that is a function of the absorbed power density are assumed:

$$D(r) = D \propto \left(P_{\mathrm{abs}}/\overline{n}_e\right)^{0.6} B_{\mathrm{ax}}^{-0.8}\,, \quad (2)$$

where P_{abs}, $\overline{n}_e$, B_{ax} are the total absorbed power, the line-averaged electron density and the magnetic field strength at the magnetic axis, respectively. The density source term S in Eq. (1) is given as the ablation profile of the pellet calculated by the neutral gas shielding (NGS) model [4]:

$$\frac{\mathrm{d}r_p}{\mathrm{d}t} \propto T_e^{1.64} n_e^{\frac{1}{3}} r_p^{-\frac{2}{3}}\,, \quad (3)$$

where r_p is the radius of the pellet. The electron temperature profile is calculated from its pressure profile and the temperature equality between electrons and ions is assumed. The electron pressure profile is estimated by a direct extrapolation of reference LHD experimental data based on gyro-Bohm type parameter dependence [5]:

$$\frac{\partial p_e(r)}{\partial t} = \frac{1}{\tau_E}\left(\gamma_{\mathrm{DPE}*}\hat{p}_e(r) P_{\mathrm{abs}}^{0.4} B^{0.8} n_e(r)^{0.6} - p_e(r)\right), \quad (4)$$

where τ_E and $\gamma_{\mathrm{DPE}*}$ are the energy confinement time, the confinement improvement factor determined by the peakedness of heating profile, respectively. The gyro-Bohm normalized electron pressure profile is defined as:

$$\hat{p}_e(r) = \frac{p_{e,\mathrm{exp}}(r)}{P_{\mathrm{abs,exp}}^{0.4} B_{\mathrm{exp}}^{0.8} n_{e,\mathrm{exp}}(r)^{0.6}} \quad (5)$$

where parameters with subscript 'exp' mean those of the reference LHD experimental data.

This reduced model can reproduce the waveform of electron density n_e, electron temperature T_e and plasma stored energy of typical

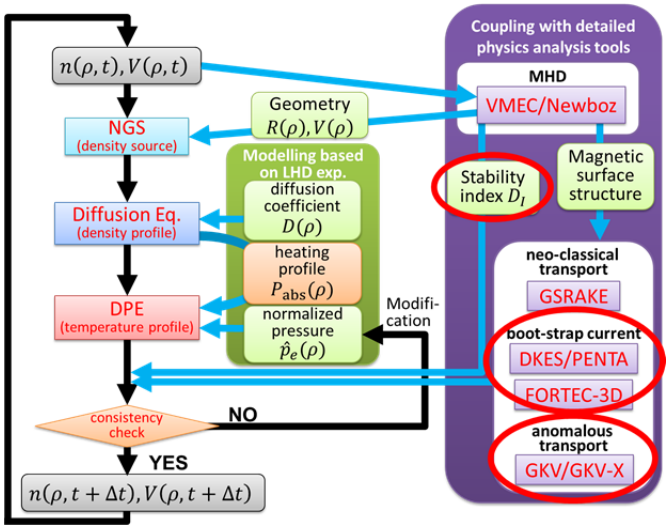

FIG. 1. Schematic of the 1-D calculations. The elements newly implemented in this study are highlighted by red circles.

pellet discharges of LHD experiment, for example, $n_e \sim 1.5\times10^{20}$ m^{-3}, $T_e \sim 2$ keV and heating power of ~ 14 MW, respectively [6]. Consistency with MHD equilibrium, MHD stability, neo-classical transport, anomalous transport and boot-strap current is examined through a direct coupling calculation with detailed physics analysis codes (MHD equilibrium and stability by VMEC [7], neo-classical transport analysis GSRAKE [8], anomalous transport by GKV/GKV-X [9] and boot-strap current by DKES/PENTA [10-12] and FORTEC-3D [13]) or the use of the model and scaling established by these codes. Figure 1 shows a schematic of the calculations.

2.2.Prerequisites of calculation

In this study, the radial profiles obtained in LHD experiment with the magnetic configuration of the inward-shifted magnetic axis position (the ratio between the magnetic axis position R_{ax} and the helical coil major radius R_c is 3.5/3.9) and high plasma aspect ratio with helical pitch parameter γ_c = 1.2 (where $\gamma_c = ma_c/(\ell R_c)$ and m, a_c, and ℓ are toroidal pitch number, helical coil minor radius and the number of helical coils, respectively) were used as the reference. The gyro-Bohm normalized electron pressure profile was fitted by a single zero-order Bessel function:

$$\hat{p}_e(\rho) = \alpha_0 J_0\left(\frac{2.4\rho}{\alpha_1}\right). \qquad (6)$$

For the initial electron density profile, the following fitting formula was used:

$$n_e(\rho) = \frac{n_{e0}}{1-\alpha_4}\left\{\left[1-\left(\frac{\rho}{\alpha_1}\right)^{\alpha_3}\right]-\alpha_4\left[1-\left(\frac{\rho}{\alpha_1}\right)^{2}\right]\right\} \qquad (7)$$

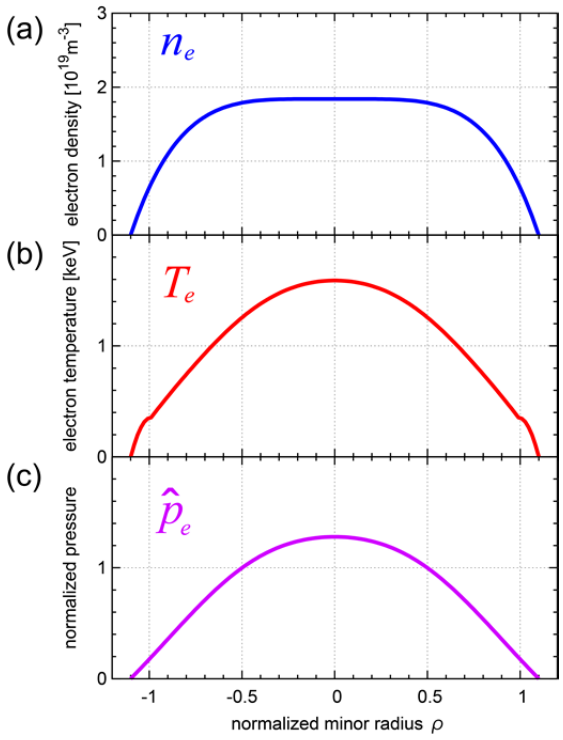

FIG. 2. Radial profiles of (a) the electron density, (b) the electron temperature, and (c) the gyro-Bohm normalized electron pressure used as the initial condition of the calculation.

The initial profiles are shown in FIG. 2. In the calculation of the diffusion equation (Eq. (1)), Dirichlet boundary condition was assumed, i.e., the electron density at the plasma boundary (corresponds to ρ = 1.1 in this case) was fixed to be zero. In the calculation of MHD equilibrium by VMEC, the shape of the last closed flux surface (LCFS) was fixed to be the same as that of the vacuum equilibrium. It has been confirmed that the shape of LCFS can be kept by adjusting the vertical magnetic field through an adequate control of the currents of the vertical field coils. Assuming electron cyclotron heating (ECH) with the frequency adjusted to the magnetic field on the axis, a Gaussian profile

$$P_{aux}(\rho) = \frac{P_{aux}}{\sqrt{2\pi\sigma^2}}\exp\left(-\frac{\rho^2}{2\sigma^2}\right) \qquad (8)$$

with σ = 0.05 was used as the power deposition profile of the external heating. The power deposition profile of alpha heating was assumed to be the same of the alpha particle birth profile calculated using the radial profiles of ion density and temperature. The absorption

coefficient of the alpha heating power is assumed to be 85% considering the result of alpha particle orbit calculation by MORH code for the high beta operation point of FFHR-d1 [14]. The density profile of helium ions was calculated by solving the diffusion equation (Eq. (1)) with the same diffusion coefficient as that of electrons. The radial profile of the effective charge was reflected in the calculation of Bremsstrahlung power loss. No other impurity was considered in the calculation. In the calculation of GSRAKE, DKES/PENTA, GKV/GKV-X and FORTEC-3D, a pure deuterium plasma was assumed and ambipolar radial electric field was self-consistently solved so that the equality of the particle flux of ions and electrons is satisfied on every flux surfaces. For the pellet fueling, the injection of a fixed size pellet (containing 2×10^{22} particles) was assumed with an injection velocity of 1.5 km/s, which can be implemented without special technological development. The minimum injection interval is set to be 5 ms considering the time resolution of the density measurement.

3. Calculation result

Using the developed 1D calculation tool, plasma operation regime of FFHR-d1B (R_c = 15.6 m, a_c = 3.744 m and magnetic field strength at R_c is 5.6 T) was examined. Here a simple control method for the pellet fueling and the external heating which can be realized with a small number of diagnostics was adopted. The injection timing of the pellet was determined by feedback control based on the line-averaged electron density. The external heating power was increased when the edge electron density (at ρ = 1.0) exceeds 0.85 times of Sudo density limit [15] and decreased when the fusion power exceeds its target value. The minimum variation range and minimum variation interval of the external heating power were set to be 1 MW and 1 sec, respectively.

As shown in FIG. 3, time evolution of critical physics parameters (e.g., Mercier index, the ratio of neo-classical energy loss to the total absorbed power) according to the change in the plasma parameters can be quantified. In LHD experiment, plasma operation regime is mainly limited by MHD instability and density limit. For the former condition, it has been observed that a low-n MHD mode which causes pressure collapse emerges when

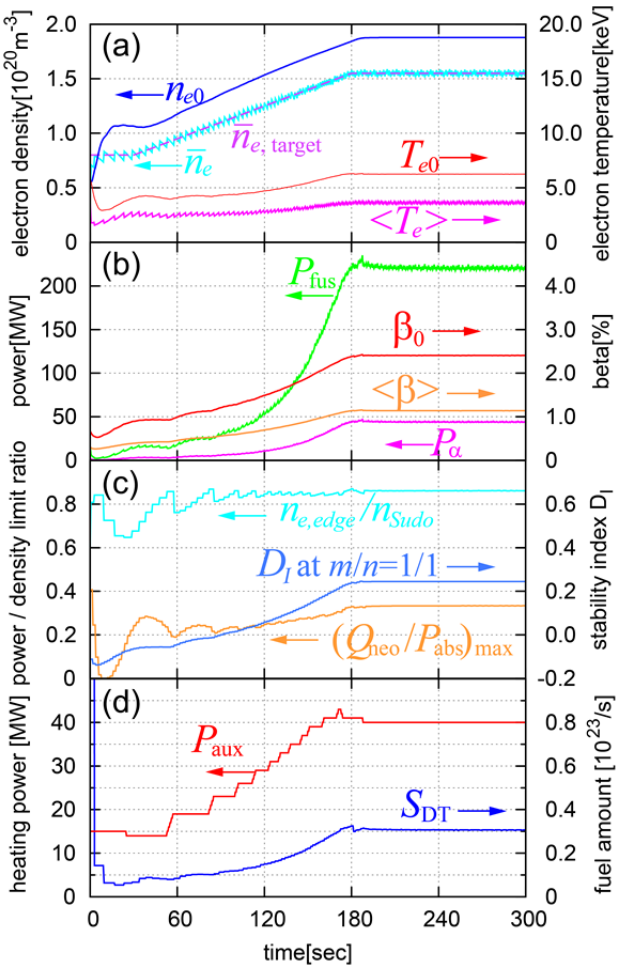

FIG. 3. Time evolution of plasma and externally controlled parameters for Q ~ 5 operation of FFHR-d1 consistent with the parameter region confirmed in LHD experiment. (a) the electron density and temperature, (b) the fusion power and beta value, (c) the neo-classical energy loss, the edge density limit and Mercier index (e) the external heating power and the injected fuel amount.

Mercier index D_I at $m/n = 1$ rational surface (corresponding to the radial position with $\iota/2\pi = 1$) exceeds 0.2–0.3. For the latter condition, it has been observed that radiation collapse occurs when the edge electron density exceeds the Sudo density limit [16]. It has also been found that the transport loss of typical LHD plasma is 2-3 times larger than the neo-classical transport loss predicted by a theory [17]. Considering these facts, it was found that a steady-state, sub-ignition operation with the fusion power of ~200 MW and the external heating power of ~40 MW (i.e., fusion gain of $Q \sim 5$) can be attained within the parameter regime that has already been confirmed in the LHD experiment. Figure 4 shows the profiles of electron density and temperature at this steady-state operation point (t = 300 s in FIG. 3). The edge electron density is less than the Sudo density limit. Figure 5 shows the radial profiles of

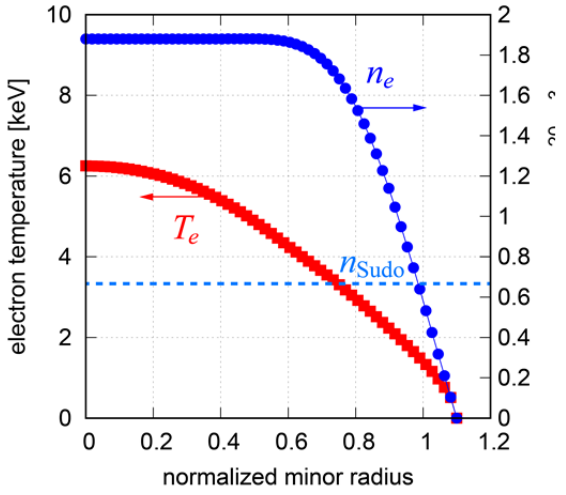

FIG. 4. Radial profiles of electron density (blue) and electron temperature (red) at the steady-state operation point with $Q \sim 5$. The value of Sudo density limit is also plotted (broken line).

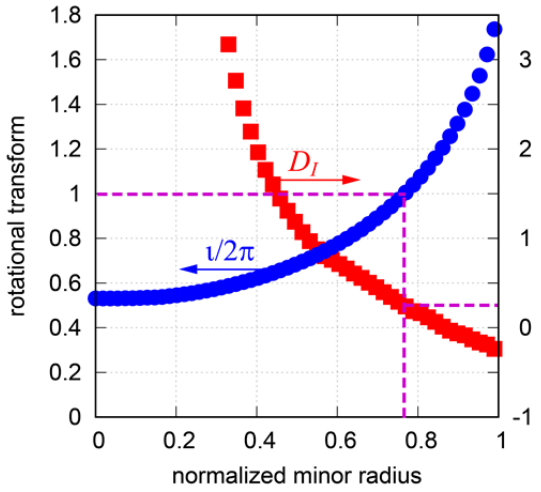

FIG. 5. Radial profiles of Mercier parameter (red) and rotational transform (blue) at the steady-state operation point with $Q \sim 5$.

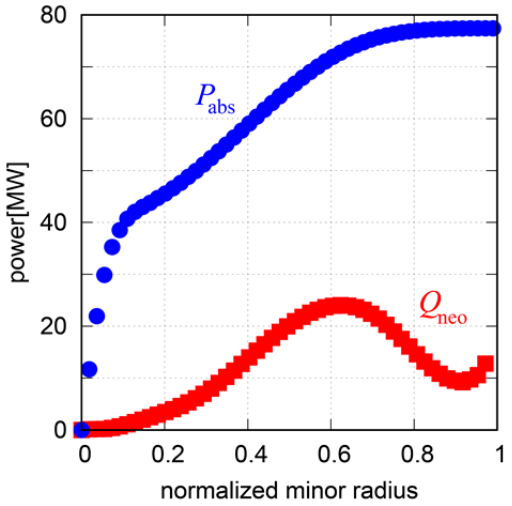

FIG. 6. Radial profiles of the integrated total neo-classical energy flux (red) and the volume integrated total absorbed power (blue) at the steady-state operation point with $Q \sim 5$.

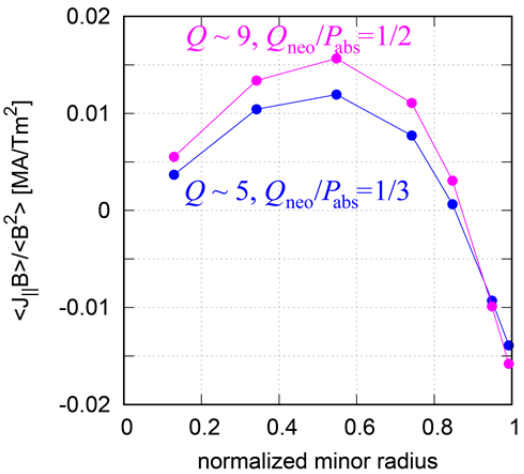

FIG. 7. Radial profile of boot-strap current at the steady-state operation point with $Q \sim 5$ (blue) and $Q \sim 9$ (magenta).

Mercier index D_I and rotational transform $\iota/2\pi$. As you can see, $D_I < 0.25$ at $\iota/2\pi = 1$ is satisfied. Figure 6 show the radial profiles of the neo-classical energy flux and the volume - integrated total absorbed power. The neo-classical energy loss is less than one-third of the total absorbed power at any radial position. Figure 7 shows the radial profiles of boot-strap current. Because the magnetic field on the axis is ~6 T, the current density of boot-strap current is less than the order of 0.1 MA/m^2 at maximum, which causes no severe change in the MHD equilibrium, i.e., radial profile of the rotational transform or the magnetic surface structure. The plasma operation contour (POPCON) plot of the steady-state operation point is shown in FIG. 8. Although the final operation point locates in thermally-unstable region (left-hand side of the saddle point), an increase of the neo-classical energy loss suppresses further increase of the electron temperature, resulting in the achievement of a steady state.

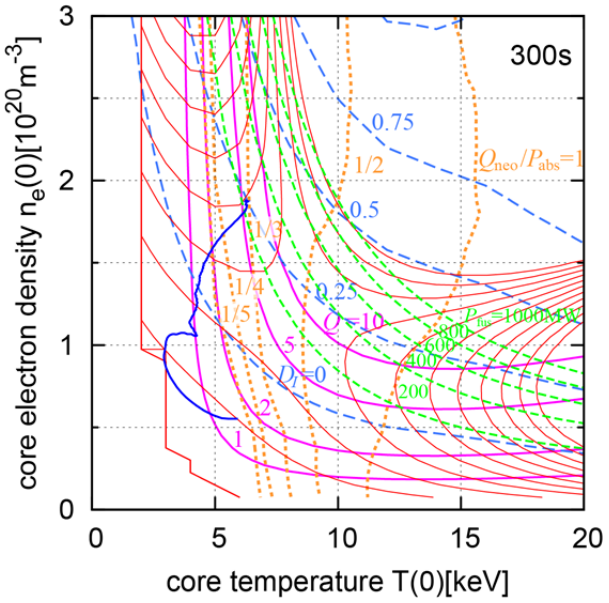

FIG. 8. POPCON plot of the steady-state operation point with the fusion gain of Q ~ 5. Red curves are the contours of the external heating power needed to sustain the plasma with the interval of 10 MW. Blue solid curve is the trajectory of electron density and temperature. Contours of fusion power (green, broken), fusion gain (magenta, solid), Mercier parameter (blue, broken) and the ratio of neo-classical energy loss to the total absorbed power (orange, dotted) are also plotted.

Assuming the conservation of the gyro-Bohm normalized electron pressure profile, the radial profiles of plasma density and temperature are virtually determined by these peak values through the pellet ablation profile. Thus, the contours of Mercier index and the ratio of neo-

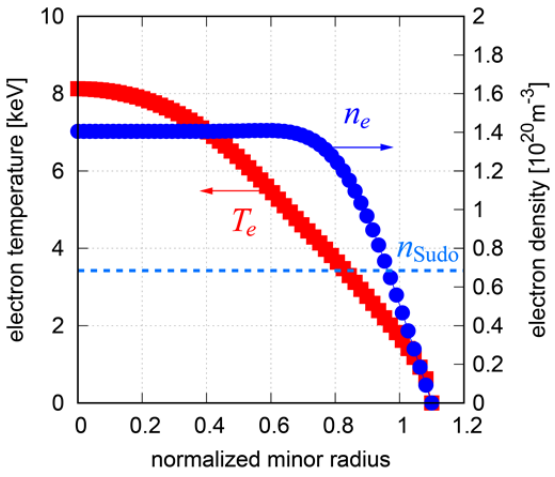

FIG. 9. Radial profiles of electron density (blue) and electron temperature (red) at the steady-state operation point with Q ~ 9. The value of Sudo density limit is also plotted (broken line).

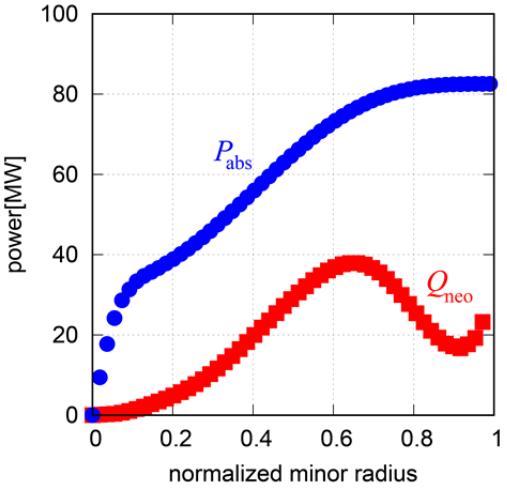

FIG. 10. Radial profiles of the integrated total neo-classical energy flux (red) and the volume integrated total absorbed power (blue) at the steady-state operation point with Q ~ 9.

classical energy loss to the total absorbed power can be plotted in the POPCON plot. Then the condition that enables higher fusion gain is clarified with a quantitative way. For example, it is found that a steady-state operation with $Q \sim 9$ (fusion power of ~300 MW with the external heating power of ~ 32 MW) is achievable if the anomalous transport is suppressed to the same level of the neo-classical transport. The radial profiles of the electron density and temperature at this $Q \sim 9$ operation point is shown in FIG. 9. The density is lower and the temperature is higher than those in the case of $Q \sim 5$. Radial profiles of the integrated total neo-classical energy flux and the volume integrated total absorbed power is shown in FIG. 10. Figure 7 shows the boot-strap current at this $Q \sim 9$ operation point does not change so much compared with the $Q \sim 5$ case. Time evolution of plasma and externally controlled parameters are shown in FIG. 11. Further increase of the fusion gain can be expected if the constraints of MHD stability and transport loss are relaxed. The operation regime can also be expanded under the same conditions if optimization of the magnetic configuration or confinement improvement is taken place. Engineering design optimization (e.g., achievement of higher magnetic field) also enables the expansion of the operation regime. In this respect, results from deuterium experiment of the LHD and the design optimization of FFHR are strongly expected to realize further attractive operation scenario.

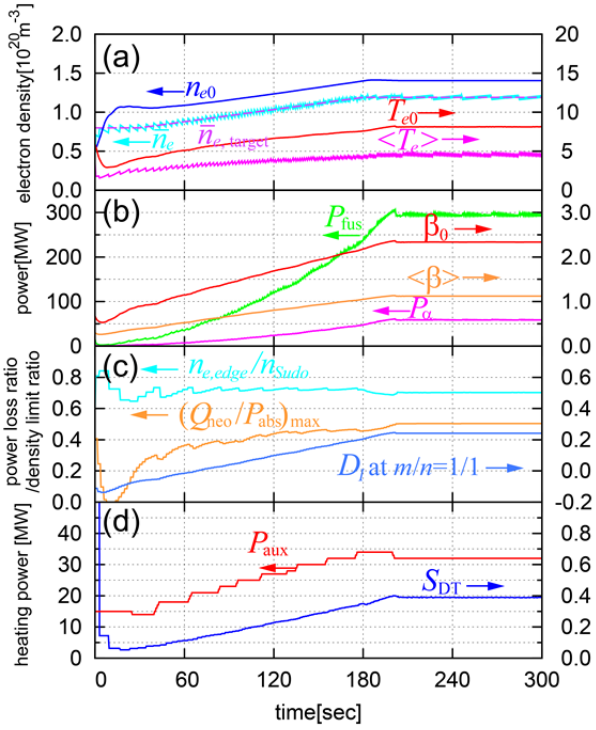

FIG. 11. Time evolution of plasma and externally controlled parameters for $Q \sim 9$ operation of FFHR-d1. (a) the electron density and temperature, (b) the fusion power and beta value, (c) the neo-classical energy loss, the edge density limit and Mercier index (e) the external heating power and the injected fuel amount.

4. Summary

The effect of the plasma and engineering design parameters on self-consistent plasma operation regime of the helical reactor FFHR-d1B was examined. It was confirmed that steady-state operation with the fusion gain of $Q \sim 5$ can be achieved within the operation regime that has been already confirmed in the LHD experiment in view of MHD equilibrium, MHD stability, neo-classical transport, anomalous transport, boot-strap current, density limit, helium impurity fraction and alpha energy loss using the 1D code coupled with detailed physics analysis codes. Although further detailed analysis including temperature inequality, the effect of the edge neutral particles and deposition profile of the heating power is needed, this study provides the direction of physics and engineering design of the LHD-type helical reactors. It also provides the design conditions of the plasma control system and contributes to the plant system design. The developed calculation tool can be a base and guidelines of the

real-time predictive simulation tool of the core plasma which aids the plasma operation control of future fusion power plants.

References

[1] SAGARA, A., et al., "Helical reactor design FFHR-d1 and c1 for steady-state DEMO", Fusion Eng. Des. **89** (2014) 2114.

[2] GOTO, T., et al., "Integrated physics analysis of plasma start-up scenario of helical reactor FFHR-d1", Nucl. Fusion **55** (2015) 063040.

[3] YOKOYAMA, M., et al., "Development of integrated transport analysis suite for LHD plasmas towards transport model validation and increased predictability", Plasma and Fusion Res. **8** (2013) 2403016.

[4] PARKS, P.B., TURNBULL, R.J., "Effect of transonic flow in the ablation cloud on the lifetime of a solid hydrogen pellet in a plasma", Phys. Fluids **21** (1978) 1735.

[5] MIYAZAWA. J., et al., "Formularization of the confinement enhancement factor as a function of the heating profile for FFHR-d1 core plasma design", Nucl. Fusion **52** (2012) 123007.

[6] SAKAMOTO, R., et al., "Operating condition to sustain burning plasma in stellarator/heliotron-type fusion reactor looking beyond LHD", Proc. of 26th Symposium on Fusion Engineering, 2015, USA, SO15-2.

[7] HIRSHMAN, S.P., et al., "Steepest-descent moment method for three-dimensional magnetohydrodynamic equilibria", Phys. Fluids **26** (1983) 3553.

[8] BEILDER, C.D., D'HAESELEER, W.D., "A general solution of the ripple-averaged kinetic equation (GSRAKE)", Plasma Phys. Control. Fusion **37** (1995) 463.

[9] NUNAMI, M., et al., "Gyrokinetic vlasov code including full three-dimensional geometry of experiments", Plasma Fusion Res. **5** (2010) 016.

[10] HIRSHMAN, S.P. et al., "Plasma transport coefficients for nonsymmetric toroidal confinement systems", Phys. Fluids **29** (1986) 2951.

[11] SPONG, D. A., "Generation and damping of neoclassical plasma flows in stellarators", Phys. Plasmas **12** (2005) 056114.

[12] SUGAMA H, NISHIMURA S., "How to calculate the neoclassical viscosity, diffusion, and current coefficients in general toroidal plasmas", Phys. Plasmas **9** (2002) 4637.

[13] SATAKE, S., et al., "Development of a non-local neoclassical transport code for helical configurations", Plasma Fusion Res. **3** (2008) S1062.

[14] MIYAZAWA. J., et al., "Physics analyses on the core plasma properties in the helical fusion DEMO reactor FFHR-d1", Nucl. Fusion **54** (2014) 043010.

[15] SUDO, S., et al., "Scalings of energy confinement and density limit in stellarator/heliotron devices", Nucl. Fusion **30** (1990) 11.

[16] MIYAZAWA, J., et al., "Density limits for the core and edge plasmas related to the local temperatures in LHD", Fusion Sci. Technol. **58** (2010) 200.

[17] YAMADA, H., et al., "Energy confinement time and heat transport in initial neutral beam heated plasmas on the Large Helical Device", Phys. Rev. Lett. **84** (2010) 1216.